RSC Advances

Effect of PMMA blend and ZnAl2O4 fillers on ionic conductivity and electrochemical performance of electrospun nanocomposite polymer blend fibrous electrolyte membrane for lithium battery

Journal:	*RSC Advances*
Manuscript ID	RA-ART-08-2015-015700.R2
Article Type:	Paper
Date Submitted by the Author:	17-Dec-2015
Complete List of Authors:	O, Padmaraj; Pondicherry University, Department of Physics M, Venkateswarlu; Amar raja Batteries, R&D N, Satyanarayana; Pondicherry University, Physics
Subject area & keyword:	Electrochemical energy < Energy

Effect of PMMA blend and $ZnAl_2O_4$ fillers on ionic conductivity and electrochemical performance of electrospun nanocomposite polymer blend fibrous electrolyte membrane for lithium battery

O. Padmaraj [a], M. Venkateswarlu [b], N. Satyanarayana [a*]

[a] Department of Physics, Pondicherry University, Pondicherry 605 014, India.

[b] R&D, Amara Raja Batteries Ltd., Karakambadi 517 520, India.

*E-mail: nallanis2011@gmail.com, **Tel:** 0413-2654 404, **fax:** +91 413 2655348

Abstract

Electrospun pure and hybrid nanocomposite PMMA blend fibrous electrolyte membranes with various *x* wt.% of $ZnAl_2O_4$, (*x* = 2, 4, 6 and 8) ceramic fillers were prepared by an electrospinning technique. All the prepared electrospun pure P(VdF-co-HFP), PMMA blend [90% P(VdF-co-HFP)/10% PMMA] and nanocomposite PMMA blend [90% P(VdF-co-HFP)/10% PMMA/*x* wt.% $ZnAl_2O_4$, (*x* = 2, 4, 6 and 8)] fibrous membranes were characterized systematically using X-ray diffraction, Fourier transform infrared spectroscopy, differential scanning calorimetry and scanning electron microscopy. The activated separator-cum nanocomposite PMMA blend fibrous electrolyte membranes were obtained by soaking in an organic liquid electrolyte solution containing 1 M $LiPF_6$ in EC: DEC (1:1, v/v). The newly developed novel nanocomposite PMMA blend fibrous electrolyte [90% P(VdF-co-HFP)/10% PMMA/6 wt.% $ZnAl_2O_4$/$LiPF_6$] membrane showed low crystallinity, high thermal stability, low average fiber diameter, high electrolyte uptake, high conductivity (4.135×10^{-3} S cm^{-1}) at room temperature and good potential stability above 4.5 V. The optimized best compositions of nanocomposite PMMA blend fibrous electrolyte membrane with 6 wt.% $ZnAl_2O_4$ fillers content is used for the fabrication of (Li/NCPBE/$LiCoO_2$) CR 2032 coin type lithium cell. The fabricated CR 2032 lithium coin cell containing the newly developed nanocomposite polymer

blend electrolyte (NCPBE) membrane delivers an initial discharge capacity of 157 mAh g^{-1} and also exhibits stable cycle performance at current density of 0.1 C - rate at room temperature.

Keywords: Electrospinning, PMMA, $ZnAl_2O_4$, NCPBE, Impedance, Charge-discharge cycles.

1. Introduction

Energy is the most essential source for our day today activities. The available fossil fuels may not be able to meet our growing energy demands. Moreover, the combustion of fossil fuels produce pollution, which cause to greenhouse effect and also fossil fuels are not renewable [1]. Many efforts have been carried out to develop pollution free, environmental friendly renewable energy sources to replace the available fossil fuels [2]. Rechargeable lithium-ion batteries are found to be more suitable with the attractive characteristics of high operating voltage, high energy density, light weight, long cycle life, environmental friendliness and it has been widely used in many portable electronic devices. Due to the unique properties, lithium-ion batteries (LIBs) will also be evolving as a best power sources in a new generation hybrid electric vehicles (HEVs), plug-in hybrids electric vehicles (PHEVs), etc. [3]. The overall cell performance of LIBs highly depends on the microstructure, electrical and electrochemical properties of the active electrode and electrolyte materials [4].

Among the various parts of the battery, an electrolyte material is an important component especially for rechargeable lithium batteries, which directly affects its electrochemical behavior such as capacity, cycle life, etc. Most of the available commercial lithium-ion batteries containing carbonate based organic liquid electrolyte, since 1990s, due to their high ionic conductivity at room temperature. But, it forces some safety issues, due to high vapor pressure, low flash point, dendrite growth formation and electrolyte leakage [5-10]. As an alternative, the use of solid polymer electrolyte has been preferred to overcome the aforementioned issues.

Solid polymer electrolytes (SPEs) have many advantages over liquid electrolytes, including: a simple design with desired size and shape, leak proof construction, resistance to shock and vibration, resistance to pressure and temperature variations, wider electrochemical stability, better safety, etc [11-15]. But, solid polymer electrolytes have low ionic conductivity ($\sim 10^{-8}$ S cm^{-1}) at room temperature as compared to organic electrolytes and it thus limits their use in conventional lithium batteries. In order to improve the ionic conductivity at room temperature, many efforts have been made to develop high conducting novel gel/composite polymer electrolytes (PEs) by adding plasticizer, polymer blend and nanocrystalline ceramic fillers [16-35].

Among these, gel polymer electrolytes (GPEs) exhibit high ionic conductivities ($\sim 10^{-3}$ S cm^{-1}) at room temperature, but their mechanical strength is not sufficient for practical applications [16-19]. Thereby, the recent attention on GPEs is thus focusing to improve their mechanical strength by adding polymer blend and nanocrystalline ceramic fillers [20-35]. Generally, the conductivity of GPEs is dominated by the quantity of absorbed liquid electrolyte, porosity and pore distribution of the polymer matrixes. GPEs are prepared by immersing the prepared porous polymer matrixes in an aprotic high dielectric constant organic solvent, which helps to dissociate the charge carriers and provides more number of ions, thereby enhancing the conductivity of the electrolyte membranes.

In GPEs, poly(vinylidene fluoride) (PVdF), poly(vinylidene fluoride-co-hexafluoroprolylene) (PVdF-co-HFP), poly (methyl methacrylate) (PMMA), poly(acrylonitrile) (PAN) and poly(styrene) (PS) have been widely used as host polymers [16-38]. Among them, P(VdF-co-HFP) copolymer is found to be a suitable promising material, as it has good electrochemical stability, affinity to electrolyte solution and high dielectric constant ($\varepsilon \approx 8.4$).

But, the crystalline part of PVdF in P(VdF-co-HFP) copolymer hinders the migration of Li^+ ions, which may lead to lower the charge/discharge capacities [37]. So, it is an importance to develop the process to modify the polymer electrolyte membranes by blending of PMMA polymer as wll as adding the nanocrystalline $ZnAl_2O_4$ ceramic particles as fillers. PMMA is a host polymer matrix for the preparation of polymer electrolytes. The PEs based on PMMA can absorb lots of liquid electrolyte, high ionic conductivity in the order of 10^{-3} Scm^{-1} at room temperature and good compatibility with the liquid electrolyte. Thereby, many researchers have been modifying by adding PMMA with another polymer matrix to improve electrolyte absorption/retention ability and the ionic conductivity of the PEs [24-25, 38-40]. The prepared nanocrystalline $ZnAl_2O_4$ ceramic fillers has strongest Lewis acid character and also having high dielectric constant (ε=8.1 - 8.3) than other fillers, which may help to form the complexes with polymer blend matrixes to improve the interfacial stability between the electrode and electrolyte.

Different methods such as solution casting, plasticizer extraction, phase inversion, hot press, electrospinning, etc., techniques have been widely used for the preparation of solid/gel polymer or nanocomposite polymer electrolyte membranes [23-41]. Among several techniques, electrospinning is a simple and an effective technique to develop thin nano/micro size porous polymer fibrous membranes with highly interconnected porous structure and large surface area, which may help to increase efficient conduction pathways for ion migration [38-44]. The PEs based on PVdF, P(VdF-co-HFP), PVdF/PMMA, PMMA-PVdF, P(VdF-co-HFP)/PMMA, P(VdF-co-HFP)/PEMA, P(VdF-co-HFP)/PMAML, PVC–PMMA, P(VdF-co-HFP)/Al_2O_3, SiO_2, TiO_2 prepared by casting, phase inversion, polymer dissolution, bellcore process and electrospinning techniques have been investigated [21-38]. Among these investigations reported, PEs prepared by an electrospinning technique has showed high ionic conductivity at room

temperature and good electrolyte uptake/retention ability compared to PEs prepared by other processes. Thus, the authors choose to develop novel nanocomposite polymer electrolytes by using an electrospinning technique, which may be a suitable electrolyte membrane for lithium-ion batteries. In our earlier studies, author's already reported that the electrospun nanocomposite polymer and polymer blend fibrous electrolyte membrane based on P(VdF-co-HFP)/ $MgAl_2O_4$ & $ZnAl_2O_4$ and P(VdF-co-HFP)/P(MMA)/$MgAl_2O_4$ have showed high ionic conductivity and good electrochemical performance at room temperature [42-44].

To the best of author's knowledge, there are no reports on the development of P(VdF-co-HFP)/PMMA/$ZnAl_2O_4$/1M $LiPF_6$ EC:DEC (1:1,v/v) nanocomposite polymer blend fibrous electrolyte membranes by an electrospinning technique. Hence, authors are motivated to develop the electrospun PMMA blend [90% P(VdF-co-HFP)/10% PMMA] and nanocomposite PMMA blend fibrous membranes [90% P(VdF-co-HFP)/10% PMMA/*x* wt.% $ZnAl_2O_4$, (*x* = 2, 4, 6 and 8 wt.%)] with the addition of various amount of nanocrystalline $ZnAl_2O_4$ ceramic particles as fillers. As prepared PMMA blend and nanocomposite PMMA blend fibrous membranes were studied systematically through different characterization techniques such as XRD, FTIR, DSC and SEM. The PMMA blend and nanocomposite PMMA blend fibrous electrolyte membranes were activated by an immersing the prepared nano/micro porous fibrous membranes in a carbonate based electrolyte solution [1M $LiPF_6$ in ethylene carbonate (EC)/diethyl carbonate (DEC) (1:1, v/v)]. The electrolyte uptake and ionic conductivities of an activated PMMA blend and nanocomposite PMMA blend fibrous electrolyte membranes are evaluated through electrolyte uptake method and impedance spectroscopy measurements at room temperature. Li/NCPBE/$LiCoO_2$ CR 2032 coin cells were assembled using the newly developed separator–cum nanocomposite PMMA blend fibrous electrolyte (NCPBE) membrane, inside an argon filled

glove box and studied their electrochemical performance using battery cycle tester (BCT) at current density of 0.1 C-rate.

2. Experimental

2.1 Materials

Poly(vinylidene difluoride-co- hexafluoropropylene) [P(VdF-co-HFP)] (Sigma Aldrich), Poly(methyl methacrylate) [PMMA] (Sigma Aldrich) and nanocrystalline $ZnAl_2O_4$ ceramic fillers, prepared by gel-combustion method, were used as precursor chemicals for the preparation of electrospun PMMA blend and nanocomposite PMMA blend fibrous membranes. Acetone and N, N-Dimethylacetamide (Ace: DMAc, 7:3, v/v) were used as solvents. 1M $LiPF_6$ in EC: DEC (1:1, v/v) (Sigma Aldrich) was used as a liquid electrolyte.

2.2 Preparation of electrospun nanocomposite PMMA blend electrolyte (NCPBE) fibrous membranes

To develop the various compositions of electrospun nanocomposite PMMA blend fibrous electrolyte membranes [90% P(VdF-co-HFP)/10% PMMA/ *x* wt.% $ZnAl_2O_4$, (*x* = 2, 4, 6 and 8)/1M $LiPF_6$]. First, an optimized 16 wt.% P(VdF-co-HFP)/PMMA (90/10) was dissolved separately in a solvent of Acetone: DMAc (7:3, v/v) under continuous stirring for 5 h at room temperature. Second, the various amount of prepared nanocrystalline *x* wt.% $ZnAl_2O_4$, (*x* = 2, 4, 6 and 8) ceramic particles were dispersed in a mixed organic solvent separately under ultrasonication. Later, the dispersed ceramic particles as fillers were slowly added to the optimized [P(VdF-co-HFP)/PMMA] blend solution under constant stirring at room temperature until to get light viscous solution. The resultant light viscous solution of each composition of nanocomposite PMMA blend was taken into a 20 ml syringe and it was loaded in a syringe pump to control the feed rate. The thin nanocomposite PMMA blend fibers were obtained by fixing an

optimized electrospinning parameters such as solution feed rate 1.5 ml h^{-1}, applied voltage between spinneret and collector is 16 kV, distance between the tip of the spinneret and collector is 15 cm, needle bore size 24 G and collector drum rotation speed is 550 rpm. The nanocomposite PMMA blend fibers were collected on the rotating drum collector to form the resultant electrospun fibrous membrane with an average thickness of 60-100 μm and further, it was dried in hot air oven at 60 °C for 24 h to remove the solvent. The fibrous PMMA blend and nanocomposite PMMA blend electrolyte membranes were prepared by soaking into a liquid electrolyte of 1M $LiPF_6$ in EC:DEC (1:1,v/v) for 30 min in a dry glove box.

2.3 Characterization techniques

X-ray diffraction (XRD) patterns were recorded from 10° to 80° for all the prepared electrospun membranes using PANalytical X-pert PRO diffractometer (Philips) with Cu-Kα radiation (λ= 0.154060 nm, 30 mA and 40 kV). Fourier transform infrared (FTIR) transmittance spectra for the prepared pure P(VdF-co-HFP), PMMA blend and nanocomposite PMMA blend fibrous membranes, were recorded in the range of 4000 to 400 cm^{-1} using NICOLET 6700 spectrophotometer with 4 cm^{-1} resolution. The DSC curves of all the prepared electrospun PMMA blend and nanocomposite PMMA blend fibrous membranes were recorded on DSC Q_{20} instrument under nitrogen atmosphere. The surface morphology of all the developed electrospun fibrous membranes was investigated, using scanning electron microscopy (SEM, Hitachi S4700). The electrolyte uptake capacity of all the electrospun membranes was determined by soaking each of them in an electrolyte solution containing 1M $LiPF_6$ in EC: DEC (1:1, v/v) and weighed it at regular intervals after removing the excess liquid electrolyte by wiping it with tissue paper. The electrolyte uptake (EU) was calculated using the following equation (Eq.1).

$$\mathrm{EU} = \frac{W_1 - W_0}{W_0} \times 100\% \quad (1)$$

where, W_1 is the mass of the wet membrane and W_0 is the mass of the dry membrane. The electrical behavior and electrochemical stability of electrospun polymer fibrous electrolyte membranes were measured using frequency response analyzer and electrochemical work station (Novocontrol, Germany). The prepared P(VdF-co-HFP)/PMMA (90/10) blend and different compositions of nanocomposite PMMA blend fibrous electrolyte membranes were sandwiched between two blocking stainless steel (SS) electrodes and the impedance spectra were recorded on Alpha high frequency response analyzer in the frequency range of 1 mHz - 1 MHz. The total conductivity of each electrospun PMMA blend and nanocomposite PMMA blend fibrous electrolyte membranes (x wt.% $ZnAl_2O_4$, x = 2, 4, 6 and 8 ceramic fillers), was calculated using the sample dimensions (thickness and area) and the resistance, evaluated from the analysis of the measured impedance data at room temperature, by using the following equation (Eq.2).

$$\sigma = \frac{t}{A \times R_b} \; S/cm \qquad (2)$$

where, t is the sample thickness (cm), A is the area (cm^2) and R_b is the bulk resistance (Ω) of each electrolyte membrane.

2.4 Electrochemical studies

The electrochemical stability of the prepared electrospun nanocomposite PMMA blend fibrous electrolyte membrane with 6 wt.% of $ZnAl_2O_4$ fillers content was studied through cyclic voltametry (Electrochemical test station POT/GAL, Novocontrol, Germany). The measurement (Li/NCPBE/SS) was carried out by using stainless steel (SS) as the working electrode and lithium (Li) metal as counter/reference electrode at the scan rate of 2 mV s^{-1} over the potential range of 2–5 V at room temperature.

For an electrochemical measurements, the CR 2032 coin type lithium cells were fabricated inside an Argon-filled glove box [Vacuum Atmospheres Co. (VAC), USA] by

sandwiching the prepared PBE or NCPBE membrane or celgard 2320 separator between lithium metal anode (380 μm thick, Aldrich) and $LiCoO_2$ cathode materials. The $LiCoO_2$ cathode active material was synthesized by a combustion method and the composite cathode was prepared by mixing 70 wt% of active material ($LiCoO_2$), 20 wt% of conducting super P carbon and 10 wt% of PVdF binder (Aldrich) in N-methyl pyrrolidinone (NMP) solvent. The resulting slurry was coated on to an Al-foil (~ 20 μm thick) using doctor blade method and dried in hot air vacuum oven at 120 °C for 24 h. The dried electrode was cut into circular disks and pressed by placing between two stainless steel (SS) plates. The charge/discharge and cycle tests of the assembled Li/PBE or NCPBE or celgard 2320/$LiCoO_2$ CR 2032 coin cells were performed at room temperature using battery cycle tester (BCT) (Model MCV4-1/0.01/0.001-10, Bitrode, USA) between the potential ranges 2.8-4.2 V at current density 0.1 C-rate.

3. Results and Discussion

The X-ray diffraction patterns of electrospun pure P(VdF-co-HFP), PMMA blend [90% P(VdF-co-HFP)/10% PMMA], nanocomposite PMMA blend fibrous membranes [90% P(VdF-co-HFP)/10% PMMA/*x* wt.% $ZnAl_2O_4$, (*x* = 2, 4, 6 and 8)] and the prepared nanocrystalline $ZnAl_2O_4$ ceramic fillers are shown in fig. 1. From fig. 1, the observed diffraction pattern of pure P(VdF-co-HFP) copolymer membrane showed one low intensity broad diffraction peak at $2\theta = 20.1^{\circ}$, which is compared with the joint committee on powder diffraction standards (JCPDS) data (Card No.00-038-1638) and confirmed the presence of PVdF crystalline phase in P(VdF-co-HFP) copolymer [31-33]. Hence, XRD results confirm the semi-crystalline nature of P(VdF-co-HFP) copolymer. The intensity of diffraction peak of PVdF is decreased drastically by an addition of 10% PMMA content in 90% P(VdF-co-HFP) copolymer, as shown in fig. 1, which confirms that the reduction of PVdF crystallinity in PMMA blend fibrous membrane. The

reduction of crystallinity indicates the formation of amorphous phase, which may be due to the reorientation of PVdF in P(VdF-HFP) chains was hindered by the large group of CH_3 OCO– in PMMA chains. Formation of amorphous structure in turn may enhance the electrolyte uptake and ionic mobility at room temperature [45-47]. Further, various contents of *x* wt.% of $ZnAl_2O_4$, (*x*=2, 4, 6 and 8) ceramic fillers were dispersed into the optimized P(VdF-co-HFP)/PMMA (90/10) blend matrix. The intensity of observed diffraction patterns of electrospun nanocomposite PMMA blend fibrous membrane is decreased upto 6 wt.% $ZnAl_2O_4$ fillers content. This indicates that the nanocomposite PMMA blend (NCPB) fibrous membranes becoming more and more amorphous nature, which may be due to the Lewis acid-base interactions between electron donor atoms in PMMA blend matrix and the cation of $ZnAl_2O_4$ ceramic fillers [43]. Further, it was confirmed from FTIR results. The amorphous nature of the NCPB fibrous membrane can provide more conducting pathways, which may help to increase the mobility (μ) of ions and hence, improves the conductivity. Also, some new diffraction peaks observed at 31.3°, 36.89° & 59.35° are compared with the $ZnAl_2O_4$ diffraction pattern and confirm the formation of $ZnAl_2O_4$ crystalline phase. Further, addition of 8 wt.% $ZnAl_2O_4$ fillers content, the intensity of diffraction peaks of nanocomposite PMMA blend fibrous membrane increases, which indicate that the $ZnAl_2O_4$ crystalline phase is increased. This may affect the mobility (μ) of free Li-ion charge carriers by blocking or hindering the path ways, which may decrease the conductivity and it was confirmed from the conductivity results.

FTIR transmittance spectra of electrospun P(VdF-co-HFP), PMMA, P(VdF-co-HFP)/PMMA (90/10) blend and nanocomposite PMMA blend fibrous membranes with an addition of $ZnAl_2O_4$ ceramic fillers content [90% P(VdF-co-HFP)/10% PMMA/*x* wt.% $ZnAl_2O_4$, (*x*=2, 4, 6 and 8)] are shown in fig. 2. The transmittance spectrum of P(VdF-co-HFP) fibrous

membrane showed strong IR bands at 1279, 842, 510 and 472 cm^{-1} are identified the characteristic peaks of PVdF ($-CH_2-CF_2-$). The bands at 1279 & 510 cm^{-1} are assigned to CF_2 asymmetric stretching and bending vibrations, respectively. The band at 842 cm^{-1} is attributed to CH_2 rocking vibration. The band at 472 cm^{-1} is assigned to CF wagging vibration [48]. In PMMA spectrum, the observed IR peaks at 1721, 1449 and 1159 cm^{-1} are assigned to C=O stretching, CH_3 stretching and $-O-CH_3$ stretching vibrations, respectively [49]. In PMMA blend [90% P(VdF-co-HFP)/10% PMMA] fibrous membrane spectrum, the observed IR vibration bands are identified both the characteristic peaks of P(VdF-co-HFP) and PMMA polymer, which reveal the perfect miscibility nature through intermolecular interactions as shown in fig. 2c [50]. The observed well defined IR bands of PMMA blend membrane spectrum become featureless broad IR bands by an addition of *x* wt.% $ZnAl_2O_4$ (*x*=2, 4, 6 and 8) fillers content of nanocomposite PMMA blend fibrous membranes as shown in fig. 2d - 2g. This attributes the formation of more amorphous nature, which is also confirmed from the observed XRD patterns of the nanocomposite PMMA blend fibrous membranes.

Figure 3 shows the DSC curves of all the electrospun P(VdF-co-HFP)/PMMA (90/10) blend and nanocomposite PMMA blend fibrous membranes with an addition of various amounts of $ZnAl_2O_4$ ceramic fillers [90% P(VdF-co-HFP)/10% PMMA/*x* wt.% $ZnAl_2O_4$, (*x* = 2, 4, 6 and 8)]. From fig.3, the DSC curve of P(VdF-co-HFP)/PMMA blend fibrous membrane exhibits two endothermic peaks at 70 $^{\circ}C$ & 140 $^{\circ}C$, corresponding to the melting or softening temperatures (T_m) of PMMA and P(VdF-co-HFP) polymers, respectively [42, 50]. This indicates that the perfect miscibility of 90% P(VdF-co-HFP) and 10% PMMA has been accomplished as a result of the possible chemical-oriented co-ordination between the '*mer*' units of the above two polymers, which confirm the better blending [50]. Moreover, it can be seen that, each curve of

nanocomposite PMMA blend fibrous membrane with the addition of various amounts of *x* wt.% $ZnAl_2O_4$ (*x*=2, 4, 6 and 8) fillers content, showed high melting temperatures at 86 °C (PMMA) & 140 °C (P(VdF-co-HFP)) as shown in fig. 3. This reflects the increase in thermal stability of nanocomposite PMMA blend fibrous membranes compared to pure P(VdF-co-HFP)/PMMA blend membrane. The increase in thermal stability of nanocomposite PMMA blend fibrous membranes is attributed to the occurrence of Lewis acid-base interactions between the incorporated nanocrystalline $ZnAl_2O_4$ fillers and P(VdF-co-HFP)/PMMA blend chains and it was confirmed from the XRD and FTIR results. Hence, the newly developed electrospun nanocomposite PMMA blend fibrous membrane with an addition of 6 wt.% $ZnAl_2O_4$ filler content [90% P(VdF-co-HFP)/10% PMMA/6 wt.% $ZnAl_2O_4$] may be a better separator-cum electrolyte membrane with good thermal stability as well as low crystallinity compared to other membranes.

Figure 4 shows the morphological SEM images of electrospun P(VdF-co-HFP) (Fig. 4a), P(VdF-co-HFP)/PMMA (90/10) blend (Fig. 4b) and nanocomposite PMMA blend fibrous membranes with an addition of various content of $ZnAl_2O_4$ ceramic fillers [*x* wt.% $ZnAl_2O_4$, (*x* = 2, 4, 6 and 8)] (Fig.4c-f). All the SEM images showed three dimensional web-like structures with fully interconnected ultrafine multi-fiber layers with uniform morphology. The interlaying of multi-fiber electrospun layers generates a nano/micro porous structure in all the developed electrospun fibrous membranes, which may be able to absorb/retain electrolyte effectively based on the porous nature [45, 51]. All the SEM images depict the variation of average fiber diameters (AFD) between the pure P(VdF-co-HFP) copolymer, P(VdF-co-HFP)/PMMA blend and nanocomposite PMMA blend fibrous membranes with various contents of *x* wt.% $ZnAl_2O_4$, (*x* = 2, 4, 6 & 8) ceramic fillers as shown in fig. 4. From the captured SEM images, the AFD of

all the electrospun membranes were measured approximately and it is found to be 1.5 μm for pure polymer, 1.75 μm for PMMA blend and nanocomposite PMMA blend fibrous membrane with various amounts of $ZnAl_2O_4$ fillers content is 0.5 μm (2wt.%), 0.5 μm (4wt.%), 0.25 μm (6wt.%) and 1 μm (8wt.%). The nanocomposite PMMA blend fibrous membrane with 6 wt.% of $ZnAl_2O_4$ fillers content exhibits less AFD (250 nm) with uniform fiber distribution compared to PMMA blend and other compositions of nanocomposite membranes. The observed difference in AFD attributes to change in the concentration of PMMA blend solution by the addition of various amounts of $ZnAl_2O_4$ ceramic fillers content. As we know that, the following spinning parameters are strongly influence the fiber diameter and morphology of fibrous membranes such as solution concentration, viscosity, feed rate, needle bore size, distance between the spinneret & collector and applied voltage. In the present work, the effect of solution concentration of P(VdF-co-HFP)/PMMA blend and the addition of various contents of $ZnAl_2O_4$ ceramic fillers were studied, while the other parameters are kept constant.

All the prepared electrospun P(VdF-co-HFP)/PMMA (90/10) blend and nanocomposite PMMA blend fibrous membranes with various contents of x wt.% $ZnAl_2O_4$, (x = 2, 4, 6 and 8) fillers were activated into separator-cum polymer electrolyte by soaking in an electrolyte solution, containing of 1M $LiPF_6$ in EC: DEC (1:1, v/v). The moment that the liquid electrolyte is dipped on the developed electrospun membranes, which spreads quickly on the surface and penetrates into the interior of the membranes within a second. This implies that the developed electrospun fibrous membranes having good porous structure and also an electron affinity between the polymer matrixes and liquid electrolyte, which may helps quick absorption/penetration of liquid electrolyte into the fibrous membranes [50].

Electrolyte uptake of the developed electrospun P(VdF-co-HFP)/PMMA blend and nanocomposite PMMA blend fibrous electrolyte membranes with various contents of *x* wt.% $ZnAl_2O_4$, (*x* = 2, 4, 6 and 8) fillers in an organic electrolyte solution as shown in fig. 5. In fig. 5, the nanocomposite polymer blend fibrous electrolyte membrane with the addition of 6 wt.% $ZnAl_2O_4$ fillers content exhibits a high electrolyte uptake up to 290% and further addition of 8 wt.% $ZnAl_2O_4$ fillers content results in a decrease of uptake behavior. The electrolyte uptake is found to increase with the addition of 10% PMMA in the polymer blend electrolyte [90% P(VdF-co-HFP)/10% PMMA/$LiPF_6$] and various amounts of $ZnAl_2O_4$ fillers content in the nanocomposite polymer blend electrolyte [90% P(VdF-co-HFP)/10% PMMA/$ZnAl_2O_4$/$LiPF_6$] membranes. This is mainly due to the excellent compatibility and affinity [P(VdF-co-HFP)/PMMA/6 wt.% $ZnAl_2O_4$] with the carbonate based liquid electrolyte in the newly developed nanocomposite polymer blend fibrous electrolyte membrane.

Figures 6 shows the complex impedance spectra of electrospun P(VdF-co-HFP)/PMMA (90/10) blend and nanocomposite PMMA blend fibrous electrolyte membranes with various contents of *x* wt.% of $ZnAl_2O_4$, (*x*=2, 4, 6 and 8) ceramic fillers at room temperature. In fig. 6, the impedance spectrum of each electrospun fibrous electrolyte membrane show one arc and an inclined spike in the measured frequency range. The observed arc in the high frequency region and the inclined spike in the low frequency region represent the bulk resistance (R_b) and double layer capacitance (C_{dl}) of the electrode/electrolyte interface effects of electrospun pure P(VdF-co-HFP)/PMMA blend and the different compositions of nanocomposite PMMA blend fibrous electrolyte membranes, respectively. The intercept of an inclined spike on the real axis (*Z*') represents the bulk resistance (R_b) of each composition of nanocomposite PMMA blend electrolyte membrane [42]. The observed impedance responses were fitted using "WinFIT"

software to evaluate the electrical response of each fibrous electrolyte membrane in the form of an equivalent circuit. The electrical conductivity (σ) of pure P(VdF-co-HFP), P(VdF-co-HFP)/PMMA (90/10) blend and each composition of nanocomposite PMMA blend fibrous electrolyte membranes were calculated using the evaluated bulk resistance (R_b) from the analyzed impedance response, sample dimensions area (A) and thickness (t). The measured bulk resistance (R_b), conductivity (σ) and electrolyte uptake of all the fibrous electrolyte membranes are given in table 1. The calculated highest conductivity of nanocomposite PMMA blend fibrous electrolyte membrane with 6 wt.% of $ZnAl_2O_4$ fillers content is found to be 4.135×10^{-3} Scm^{-1} at room temperature.

The variation of electrical conductivity and electrolyte uptake with respect to the addition of various contents of x wt.% $ZnAl_2O_4$, (x = 2, 4, 6 and 8) ceramic fillers into the P(VdF-co-HFP)/PMMA (90/10) blend fibrous electrolyte membranes are shown in fig. 5. In fig. 5, the electrical conductivity increases with an addition of $ZnAl_2O_4$ ceramic fillers content up to 6 wt.%, which may be due to the formation of more conduction pathways in the amorphous phase, allowing greater Li-ion migration and more electrolyte absorption [42-44]. Further, addition of 8 wt.% of $ZnAl_2O_4$ ceramic fillers content results in decrease of electrical conductivity, which may be due to the formation of agglomerated $ZnAl_2O_4$ particles. The agglomerated $ZnAl_2O_4$ particles may lead to block or hinder the migration of Li-ions in the nanocomposite PMMA blend electrolyte membranes. The complete mechanism of the nanocomposite PMMA blend fibers with various amounts of $ZnAl_2O_4$ ceramic fillers and an activated nanocomposite polymer blend electrolyte fiber is shown in fig. 7, in the form of schematic diagrams. Hence, the optimized nanocomposite PMMA blend fibrous electrolyte membrane with 6 wt.% of $ZnAl_2O_4$ fillers

content can be swollen sufficiently with the carbonate-based liquid electrolyte, which lead to increase the ionic conductivity at room temperature.

The potential stability window of the optimized high conductivity composition of electrospun nanocomposite PMMA blend fibrous electrolyte membrane with 6 wt.% of $ZnAl_2O_4$ ceramic fillers at room temperature is shown in fig. 8. The observed steady increase in current with respect to applied voltage indicates the potential stability limit of the electrolyte membrane [44]. In fig. 8, it can be found that, the optimized electrospun nanocomposite PMMA blend fibrous electrolyte membrane with 6 wt.% of $ZnAl_2O_4$ fillers content exhibits high stability above ~ 4.5 V. Hence, the newly developed high potential stability limit of nanocomposite PMMA blend fibrous electrolyte membrane should render them potentially compatible with the most high voltage cathode materials for high energy density rechargeable lithium batteries.

Figure 9 shows a comparative charge-discharge curves of CR 2032 lithium cells containing the optimized nanocomposite PMMA blend separator-cum fibrous electrolyte membrane with 6 wt.% of $ZnAl_2O_4$ fillers content at a current density of 0.1 C-rate. From fig. 9, the discharge capacity of nanocomposite PMMA blend fibrous electrolyte membrane is found to be 157 mAh g^{-1} for 1^{st} cycle and 132 mAh g^{-1} for 30^{th} cycle. The observed capacity difference from 1^{st} to 30^{th} cycles of assembled CR 2032 Li/NCPBE/$LiCoO_2$ cell, showed an approximately 25 mAh g^{-1}, which is probably due to the difference in Li-ion conductivity and utilization of active material. The optimized electrospun nanocomposite PMMA blend electrolyte membrane has high porosity with ultra-fine pore structure, which might have absorbed large amount of liquid electrolyte as compared to commercial available celgard separators [42-44]. This may help to enhance the ionic conductivity by entrap the Li ions into the separator-cum nanocomposite polymer blend electrolyte fibrous membrane, which indicate the higher

utilization of active material by sustains the absorbed electrolyte through charge/discharge process.

Figure 10 shows the discharge capacity as a function of cycle number for the fabricated CR 2032 Li/$LiCoO_2$ cell using the optimized electrospun nanocomposite PMMA blend separator-cum fibrous electrolyte membrane with 6 wt.% of $ZnAl_2O_4$ ceramic fillers content at room temperature. From fig.10, the discharge capacity of 1^{st} and 30^{th} cycle of Li/NCPBE/$LiCoO_2$ cell shows 157 mAh g^{-1} and 132 mAh g^{-1} respectively. The observed capacity fade may be due to the structural characteristics and composition of cathode material, which plays a vital role on the capacity of cell and cycling performance. Hence, the electrospun nanocomposite PMMA blend separator-cum fibrous electrolyte membrane with 6 wt.% of $ZnAl_2O_4$ fillers content has good cycle performance without any change in the property, which confirms the excellent efficiency of the electrolyte membrane to conduct the ions between the electrodes. Also, it has good compatibility with both the electrodes especially lithium metal. Thus, it may be concluded that the newly developed nanocomposite PMMA blend fibrous electrolyte membrane [90% P(VdF-co-HFP)/10% PMMA/6 wt.% $ZnAl_2O_4$/1 M $LiPF_6$, EC:DEC (1:1,v/v)] can be useful as a better separator-cum polymer electrolyte for all rechargeable lithium battery application as well as other ionic devices.

4. Conclusion

The optimized electrospun P(VdF-co-HFP)/PMMA (90/10) blend and nanocomposite PMMA blend fibrous membranes with various contents of $ZnAl_2O_4$ ceramic fillers [90% P(VdF-co-HFP)/10% PMMA/x wt.% $ZnAl_2O_4$, (x = 2, 4, 6 and 8)] were prepared by simple electrospinning technique. The nanocomposite PMMA blend membrane with 6 wt.% of $ZnAl_2O_4$ fillers content showed the reduction of PVdF crystallinity, low average fiber diameter

with uniform morphology, good thermal stability and high electrolyte uptake. The activated nanocomposite PMMA blend fibrous electrolyte membranes [90% P(VdF-co-HFP)/10% PMMA /6 wt.% $ZnAl_2O_4$/1M $LiPF_6$] showed high ionic conductivity with good electrochemical stability at room temperature. The fabricated CR 2032 Li/NCPBE/$LiCoO_2$ coin cell using the optimized the high conductivity composition of nanocomposite PMMA blend fibrous electrolyte membranes with 6 wt.% of $ZnAl_2O_4$ fillers content delivers the good charge-discharge capacity and also exhibits stable cycle performance at room temperature. Hence, the newly developed electrospun nanocomposite PMMA blend fibrous electrolyte membrane can be used as a separator-cum polymer electrolyte membrane for high performance rechargeable lithium batteries as well as other electrochemical device applications.

Acknowledgements

Dr. NS is gratefully acknowledges to DST, AICTE, UGC, CSIR, BRNS-DAE and DRDO, Govt. of India, for financial support through major research project grants. O.P is thankful to UGC for the award of BSR fellowship for pursuing the doctoral degree. Authors also acknowledge CIF, Pondicherry University, for providing DSC & SEM facilities.

References

1 M. Armand, J.M. Tarascon, *Nature*, 2008, **451**, 652-657.

2 J.B. Goodenough, Y. Kim, *Chem. Mater*., 2010, **22**, 587-603.

3 L. Su, Y. Jing, Z. Zhou, *Nanoscale*, 2011, **3**, 3967-3983.

4 M. Hu, X. Pang, Z. Zhou, *J. Power Sources*, 2013, **237**, 229-242.

5 K. Xu, *Chem. Rev*., 2004, **104**, 4303–4417.

6 Yu Wang, Wei-Hong Zhong, *Chem. Electro Chem*., 2015, **2**, 22–36.

7 Kang Xu, *Chem. Rev*., 2014, **114**, 11503−11618.

8 M. Ue, S. Mori, *J. Electrochem. Soc*., 1995, **142**, 2577–2581.

9 M. Schmidta, U. Heidera, A. Kuehnera, R. Oestena, M. Jungnitza, N. Ignatevb, P. Sartorib, *J. Power Sources*, 2001, **97/98**, 557–560.

10 C.W. Walker Jr., J.D. Cox, M. Salomon, *J. Electrochem. Soc*., 1996, **143**, L80-L82.

11 J. Xi, X. Qiu, J. Li, X. Tang, W. Zhu, L. Chen, *J. Power Sources*, 2006, **157**, 501.

12 Eliana Quartarone, Piercarlo Mustarelli, *Chem. Soc. Rev*., 2011, **40**, 2525–2540.

13 Zhigang Xue, Dan He, Xiaolin Xie, *J. Mater. Chem. A*, 2015, **3**, 19218–19253.

14 M. Park, X. Zhang, M. Chung, G. B. Less, A. M. Sastry, *J. Power Sources*, 2010, **195**, 7904-7929.

15 Vijay Kumar Thakur, Guoqiang Ding, Jan Ma , Pooi See Lee , Xuehong Lu, *Adv. Mater*., 2012, **24**, 4071–4096.

16 J.Y. Song, Y.Y.Wang, C.C.Wan, *J. Power Sources*, 1999, **77**, 183-197.

17 M. Stephen, *Eur. Pol. J*., 2006, **42**, 21–42.

18 R. Koksbang, I.I. Olsen, D. Shackle, *Solid State Ionics*, 1994, **69**, 320-335.

19 Mariusz Walkowiaka, Aldona Zalewska, Teofil Jesionowski, Monika Pokora, *J. Power Sources*, 2007, **173**, 721–728.

20 S. Rajendiran, R. Kannan, O. Mahendran, *J. Power Sources*, 2001, **96**, 406-410.

21 Zhan-liang Wang, Zhi-yuan Tang, *Electrochim. Acta*, 2004, **49**, 1063–1068.

22 L.N. Sim, S.R. Majid, A.K. Arof, *Solid State Ionics*, 2012, **209–210**, 15–23.

23 Isabella Nicotera, Luigi Coppola, Cesare Oliviero, Marco Castriota, Enzo Cazzanelli, *Solid State Ionics*, 2006, **177**, 581–588.

24 Dar-Jong Lin, Chi-Lin Chang, Chih-Kang Lee, Liao-Ping Cheng, *Eur. Poly. J.*, 2006, **42**, 2407–2418.

25 A. Subramania, N.T. Kalyana Sundaram, A.R. Sathiya Priya, G. Vijaya Kumar, *J. Memb. Sci.*, 2007, **294**, 8–15.

26 Cui Zhen-Yu, Xu You-Yi, Zhu Li-Ping, Wang Jian-Yu, Xi Zhan-Yu, Bao-Ku-Zhu., *J. Memb. Sci.*, 2008, **325**, 957-963.

27 A. Manuel Stephen, K.S. Nahm, *Polymer*, 2006, **47**, 5952-5964.

28 Choi Byoung-Koo, Kim Young-Wan, Shin. Kyoung-Hee, *J. Power Sources*, 1997, **68**, 357-360.

29 S. Jung, D.W. Kim, S.D. Lee, M. Cheong, D.Q. Nguyen, B.W. Cho, H. S. Kim, *Bull. Korean Chem. Soc*., 2009, **30**, 2355-2361.

30 A. Sarnowska, I. Polska, L. Niedzicki, M. Marcinek, A. Zalewska, *Electrochim. Acta*, 2011, **57**, 180– 186.

31 F. Croce, R. Curini, A. Martinelli, L. Persi, F. Ronci, B. Scrosati, R. Caminiti, *J. Phys. Chem. B*, 1999, **103**, 10632-10638.

32 G. Derrien, J. Hassoun, S. Sacchetti, S. Panero, *Solid State Ionics*, 2009, **180**, 1267–1271.

33 F. Croce, G. B. Appetecchi, L. Persi, B. Scrosati, *Nature*, 1998, **394**, 456-458.

34 J.E. Weston, B.C.H. Steele, *Solid State Ionics*, 1982, **7**, 75-79.

35 Kun Gao, Xinguo Hu, Chongsong Dai, Tingfeng Yi, *Mater. Sci. and Eng. B*, 2006, **131**, 100–105.

36 Jae-Kwang Kim, Gouri Cheruvally, Xin Li, Jou-Hyeon Ahn, Ki-Won Kim, Hyo-Jun Ahn, *J. Power Sources*, 2008, **178**, 815–820.

37 Raghavan Prasanth, Vanchiappan Aravindan, Madhavi Srinivasan, *J. Power Sources*, 2012, **202**, 299 – 307.

38 Zheng Zhong, Qi Cao, Xianyou Wang, Na Wu, Yan Wang, *Ionics*, 2012, **18**, 47–53.

39 G. Appetecchi, F. Croce, B. Scrosati, *Electrochim. Acta*, 1995, **40**, 991.

40 H. Rhoo, H.T. Kim, J.K. Park, T.S. Hwang, *Electrochim. Acta*, 1997, **42**, 1571.

41 Ding Yanhuai, Zhang Ping, Long Zhilin, Jiang Yong, Fu Xu, Di. Wei, *J. Memb. Sci.*, 2009, **329**, 56-59.

42 O. Padmaraj, B. Nageswara Rao, Paramananda Jena, M. Venkateswarlu, N. Satyanarayana, *Polymer*, 2014, **55**, 1136 -1142.

43 O. Padmaraj, M. Venkateswarlu, N. Satyanarayana, *Electroanalysis*, 2014, **26**, 1 – 8.

44 O. Padmaraj, B. Nageswara Rao, M. Venkateswarlu, N. Satyanarayana, *J. Phys. Chem. B*, 2015, **119**, 5299−5308.

45 Y. Liang, S. Cheng, J. Zhao, C. Zhang, S. Sun, N. Zhou, Y. Qiu, X. Zhang, *J. Power sources*, 2013, **240**, 204-211.

46 Li. Xiaoyun, Cao Qi, Wang Xianyou, Jiang Shenghui, Deng Huayang, Wu. Na, *J. Appl. Poly. Sci.*, 2011, **122**, 2616–2620.

47 Kwang Man Kim, Nam-Gyu Park, Kwang Sun Ryu, Soon Ho. Chang, *Polymer*, 2002, **43**, 3951-3957.

48 V. Aravindan, P. Vickraman, *J. Renew. Sustain. Ener.*, 2009, **1**, 023108-1-023108-11.

49 S. Ramesh, Koay Hang Leen, K. Kumutha, A.K. Arof, *Spectrochim. Acta Part A*, 2007, **66**, 1237–1242.

50 Cui Wei-Wei, Tang Dong-Yan, Gong Zai-Lin, *J. Power sources*, 2013, **223**, 206-213.

51 Jae-Kwang Kim, Gouri Cheruvally, Zin Li, Jou-Hyeon Ahn, Ki-Won Kim, Hyo-Jun Ahn, *J. Power sources*, 2008, **178**, 815-820.

Table 1 Electrical properties and electrolyte uptake of electrospun pure P(VdF-co-HFP), P(VdF-co-HFP)/PMMA (90/10) blend and nanocomposite PMMA blend fibrous electrolyte membranes with various contents of $ZnAl_2O_4$ ceramic particles as fillers.

S. No	Samples	Resistance (R_b) Ω	Conductivity (σ) S cm^{-1}	EU* (%)
1	Pure P(VdF-co-HFP)	38.7	1.875×10^{-4}	52
2	90% P(VdF-co-HFP)/10%PMMA	4.40	1.788×10^{-3}	58
3	90% P(VdF-co-HFP)/10%PMMA/2 wt.% $ZnAl_2O_4$	2.65	3.004×10^{-3}	70
4	90% P(VdF-co-HFP)/10%PMMA/4 wt.% $ZnAl_2O_4$	2.45	3.069×10^{-3}	127
5	90% P(VdF-co-HFP)/10%PMMA/6wt.% $ZnAl_2O_4$	2.65	4.135×10^{-3}	290
6	90% P(VdF-co-HFP)/10%PMMA/8 wt.% $ZnAl_2O_4$	3.95	2.842×10^{-3}	160

***EU: Electrolyte Uptake**

Figure Captions

1. **Fig. 1** X-ray diffraction patterns of electrospun pure P(VdF-co-HFP), P(VdF-co-HFP)/PMMA blend (90/10) and nanocomposite PMMA blend fibrous membranes with various contents of *x* wt% $ZnAl_2O_4$, (*x* =2, 4, 6 and 8) ceramic fillers.
2. **Fig. 2** FTIR spectra of electrospun a) pure P(VdF-co-HFP), b) pure PMMA, c) P(VdF-co-HFP)/PMMA blend (90/10) and d-g) nanocomposite PMMA blend fibrous membranes with various contents of *x* wt% $ZnAl_2O_4$, (*x* =2, 4, 6 and 8) ceramic fillers.
3. **Fig. 3** DSC curves of electrospun P(VdF-co-HFP)/PMMA (90/10) blend and nanocomposite PMMA blend fibrous membranes with various contents of *x* wt% $ZnAl_2O_4$, (*x* =2, 4, 6 and 8) ceramic fillers.
4. **Fig. 4** SEM images of electrospun a) pure P(VdF-co-HFP), b) P(VdF-co-HFP)/PMMA (90/10) blend and nanocomposite PMMA blend fibrous membranes with various contents of *x* wt% $ZnAl_2O_4$, (*x* =2, 4, 6 and 8) ceramic fillers c) 2 wt% $ZnAl_2O_4$, d) 4 wt% $ZnAl_2O_4$, e) 6 wt% $ZnAl_2O_4$ and f) 8 wt% $ZnAl_2O_4$.
5. **Fig. 5** Variation of electrical conductivity (red colour line) and absorbed liquid electrolyte (black colour line) of electrospun P(VdF-co-HFP)/PMMA (90/10) blend and nanocomposite PMMA blend fibrous electrolyte membranes with various contents of *x* wt% $ZnAl_2O_4$, (*x* =2, 4, 6 and 8) ceramic fillers at room temperature.
6. **Fig. 6** Complex impedance spectra of real and imaginary parts of electrospun P(VdF-co-HFP)/PMMA (90/10) blend and nanocomposite PMMA blend fibrous electrolyte membranes with various contents of *x* wt% $ZnAl_2O_4$, (*x* =2, 4, 6 and 8) ceramic fillers at room temperature.
7. **Fig. 7** Schematic diagram for the complete mechanism of the nanocomposite PMMA blend fibers with various amounts of $ZnAl_2O_4$ ceramic fillers and an activated nanocomposite polymer blend electrolyte fiber with an organic liquid electrolyte containing 1M $LiPF_6$ EC:DEC (1:1, v/v).
8. **Fig. 8** Potential stability window of the electrospun nanocomposite PMMA blend fibrous electrolyte membrane with 6 wt.% of $ZnAl_2O_4$ fillers content at room temperature.
9. **Fig. 9** Charge-discharge capacity of Li/NCPBEs/$LiCoO_2$ CR 2032 coin cell containing the optimized electrospun nanocomposite PMMA blend fibrous electrolyte membrane with 6 wt.% of $ZnAl_2O_4$ fillers content at room temperature.

10. **Fig. 10** Cycle performance of Li/NCPBEs/$LiCoO_2$ CR 2032 coin cell containing the optimized electrospun nanocomposite PMMA blend fibrous electrolyte membranes with 6 wt.% of $ZnAl_2O_4$ fillers content at room temperature.

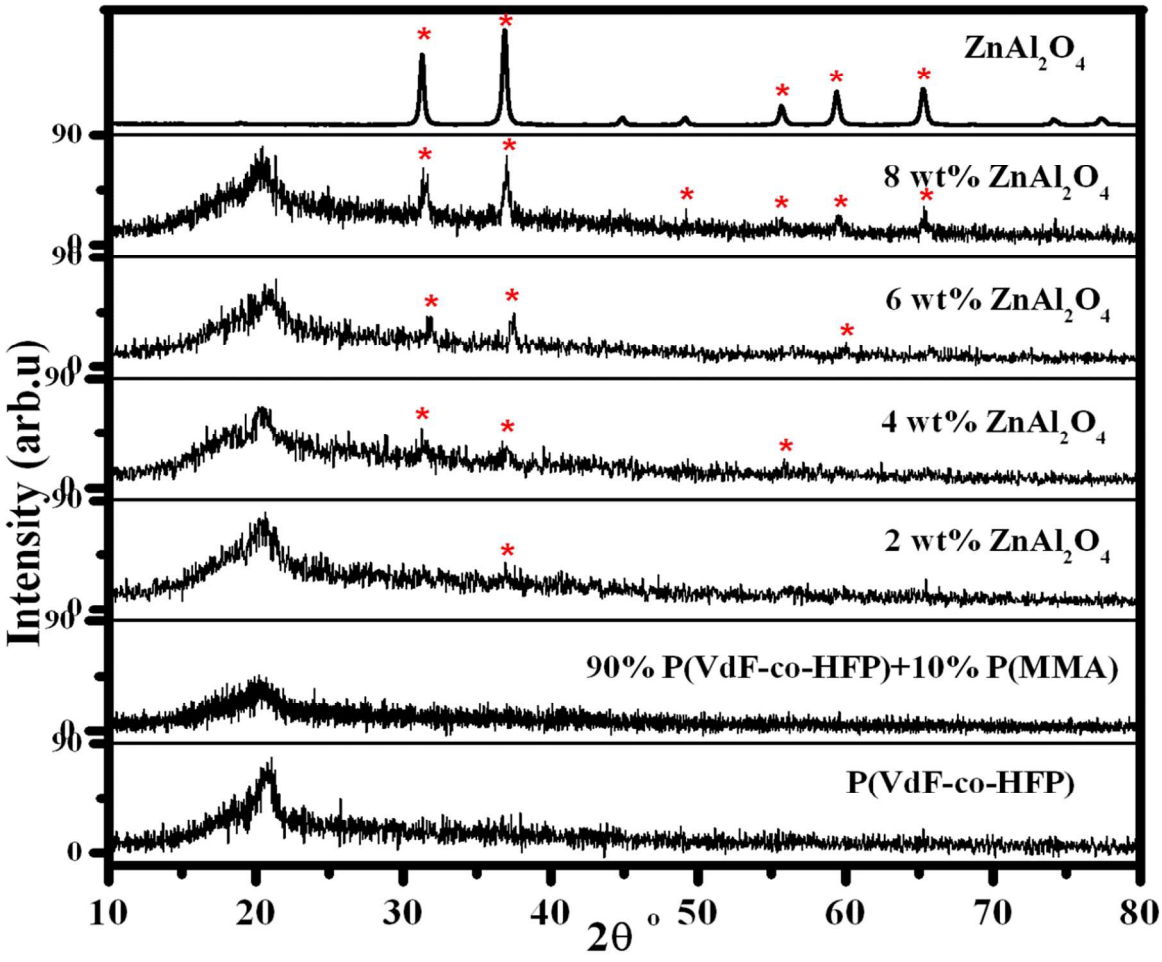

Fig. 1 X-ray diffraction patterns of electrospun pure P(VdF-co-HFP), P(VdF-co-HFP)/PMMA blend (90/10) and nanocomposite PMMA blend fibrous membranes with various contents of *x* wt% $ZnAl_2O_4$, (*x* =2, 4, 6 and 8) ceramic fillers.

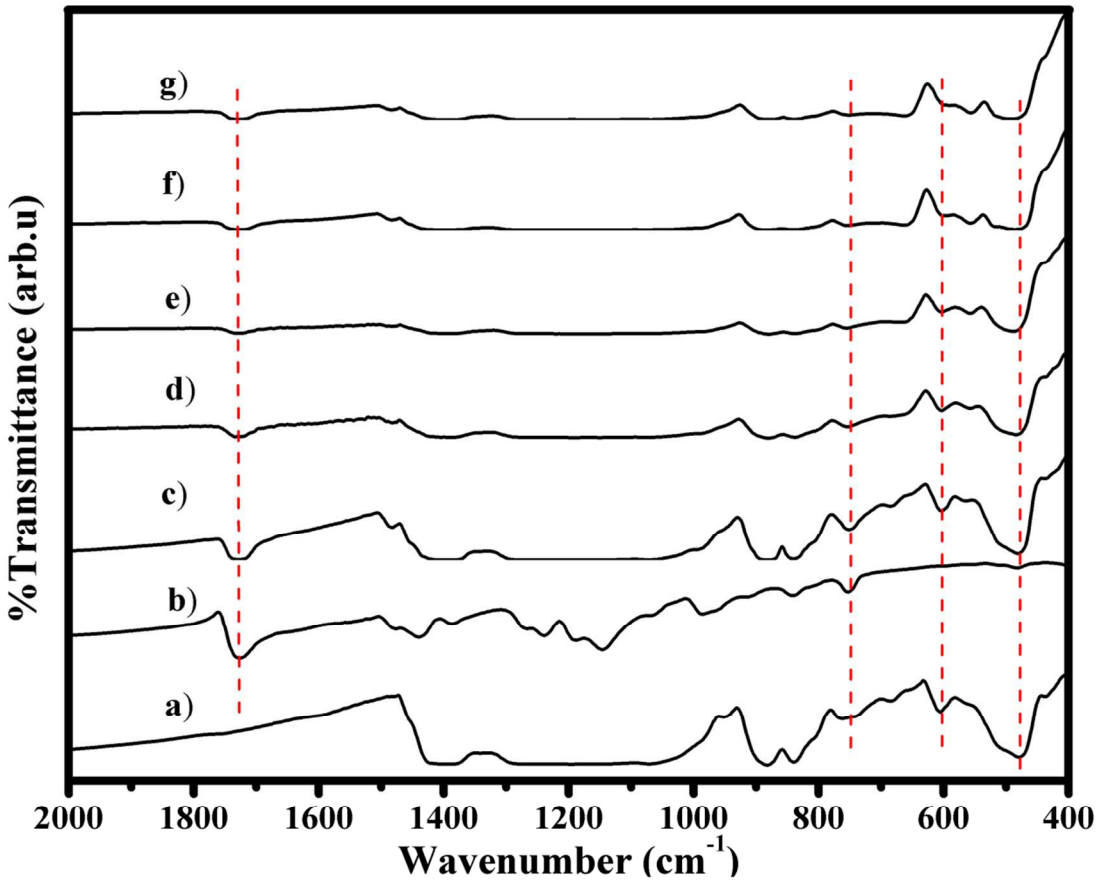

Fig. 2 FTIR spectra of electrospun a) pure P(VdF-co-HFP), b) pure PMMA, c) P(VdF-co-HFP)/PMMA blend (90/10) and d-g) nanocomposite PMMA blend fibrous membranes with various contents of *x* wt% $ZnAl_2O_4$, (*x* =2, 4, 6 and 8) ceramic fillers.

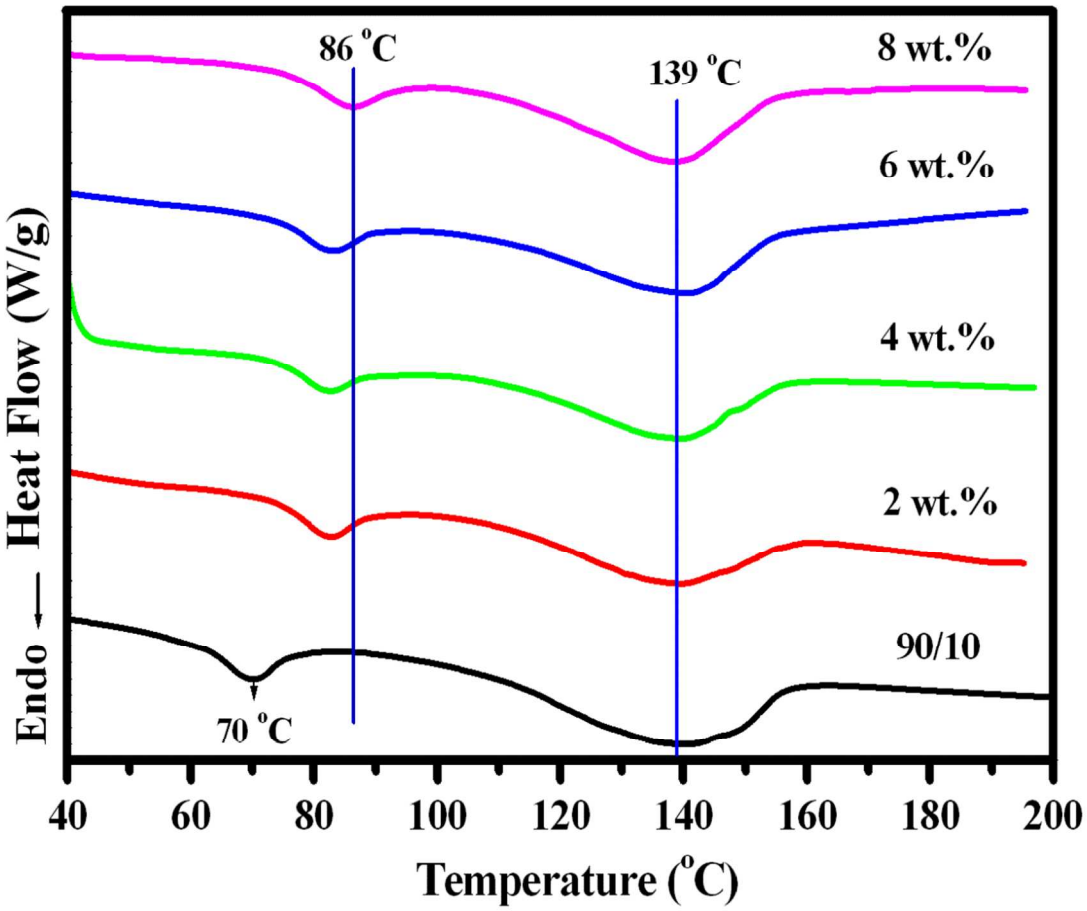

Fig. 3 DSC curves of electrospun P(VdF-co-HFP)/PMMA (90/10) blend and nanocomposite PMMA blend fibrous membranes with various contents of *x* wt% $ZnAl_2O_4$, (*x* =2, 4, 6 and 8) ceramic fillers.

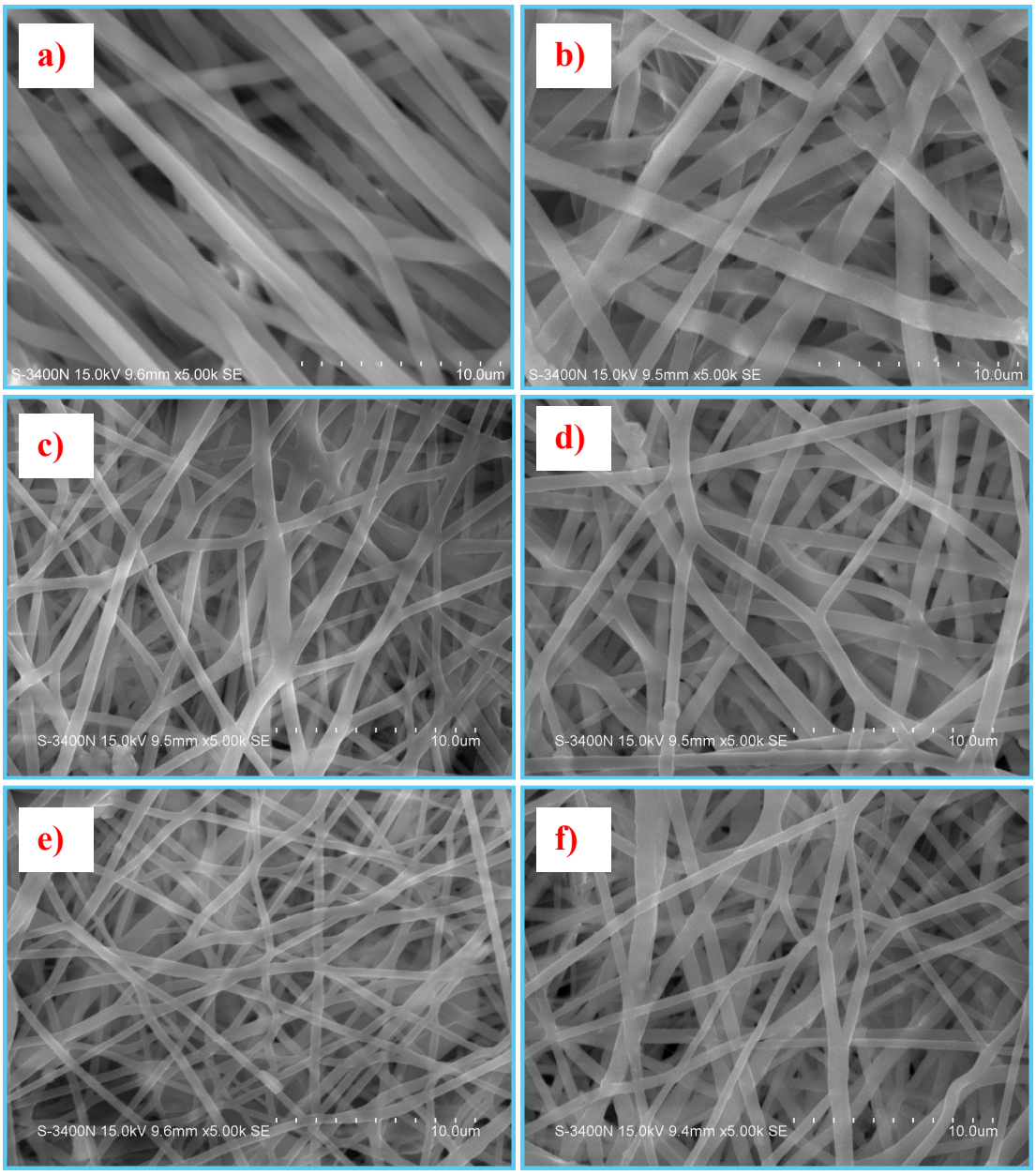

Fig. 4 SEM images of electrospun a) pure P(VdF-co-HFP), b) P(VdF-co-HFP)/PMMA (90/10) blend and nanocomposite PMMA blend fibrous membranes with various contents of *x* wt% $ZnAl_2O_4$, (*x* =2, 4, 6 and 8) ceramic fillers c) 2 wt% $ZnAl_2O_4$, d) 4 wt% $ZnAl_2O_4$, e) 6 wt% $ZnAl_2O_4$ and f) 8 wt% $ZnAl_2O_4$.

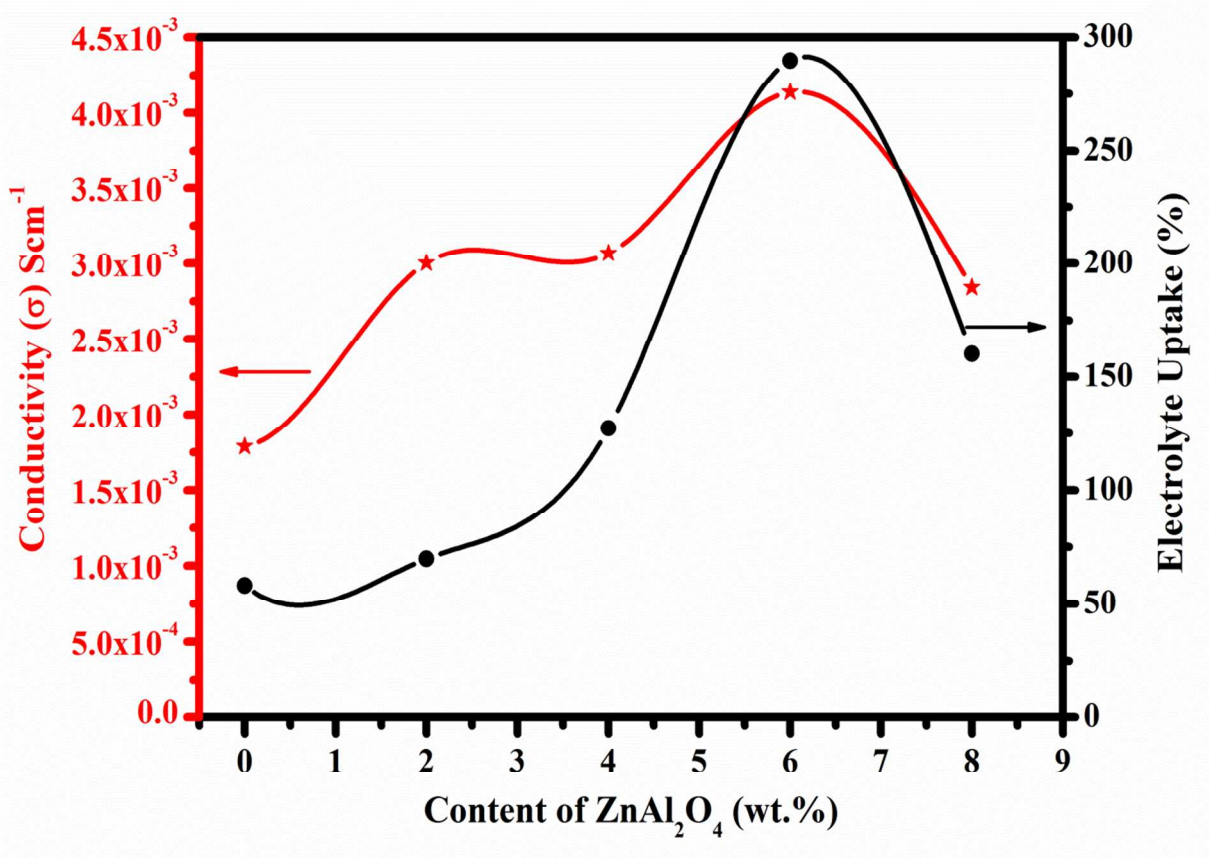

Fig. 5 Variation of electrical conductivity (red colour line) and absorbed liquid electrolyte (black colour line) of electrospun P(VdF-co-HFP)/PMMA (90/10) blend and nanocomposite PMMA blend fibrous electrolyte membranes with various contents of *x* wt% $ZnAl_2O_4$, (*x* =2, 4, 6 and 8) ceramic fillers at room temperature.

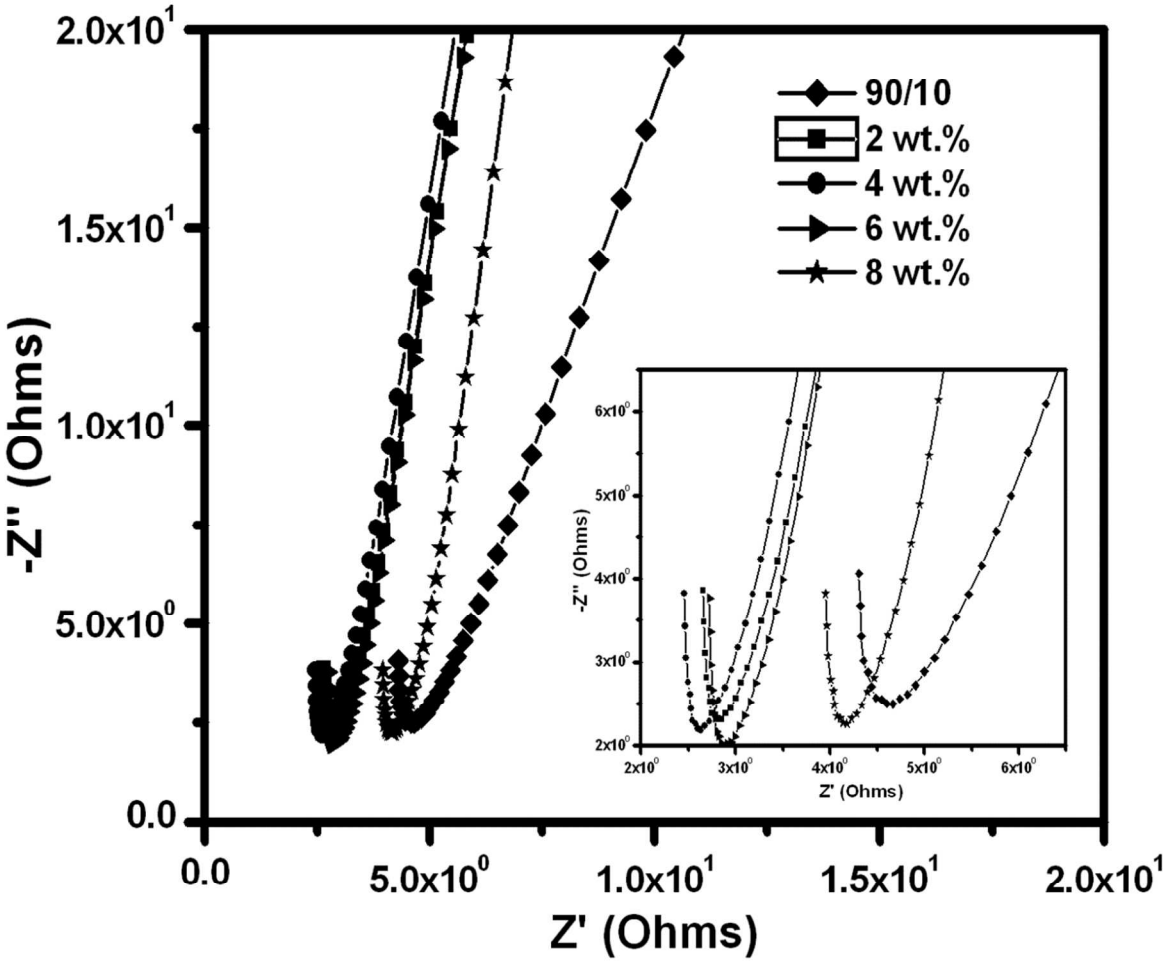

Fig. 6 Complex impedance spectra of real and imaginary parts of electrospun P(VdF-co-HFP)/PMMA (90/10) blend and nanocomposite PMMA blend fibrous electrolyte membranes with various contents of *x* wt% $ZnAl_2O_4$, (*x* =2, 4, 6 and 8) ceramic fillers at room temperature.

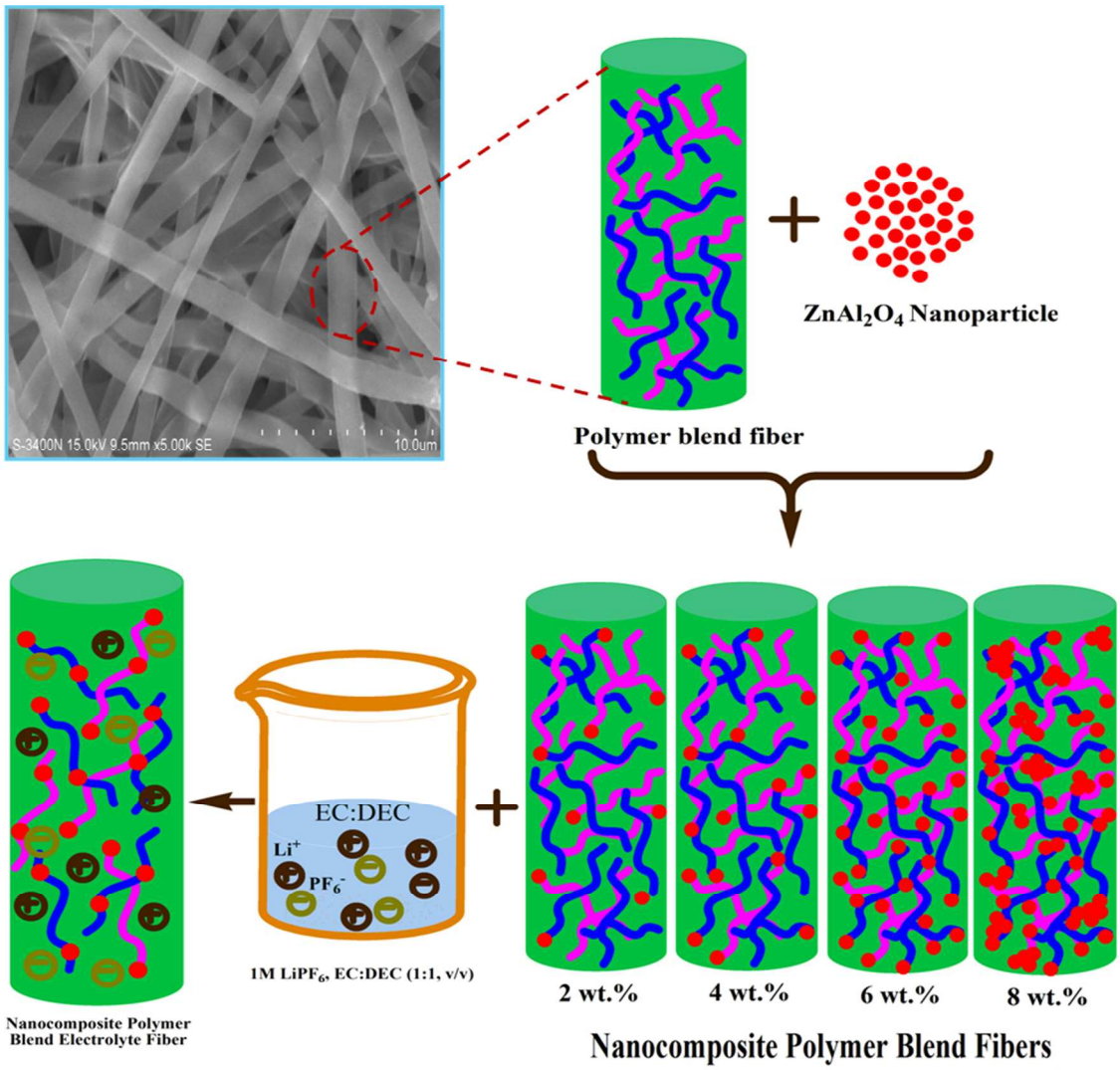

Fig. 7 Schematic diagram for the complete mechanism of the nanocomposite PMMA blend fibers with various amounts of $ZnAl_2O_4$ ceramic fillers and an activated nanocomposite polymer blend electrolyte fiber with an organic liquid electrolyte containing 1M $LiPF_6$ EC:DEC (1:1, v/v).

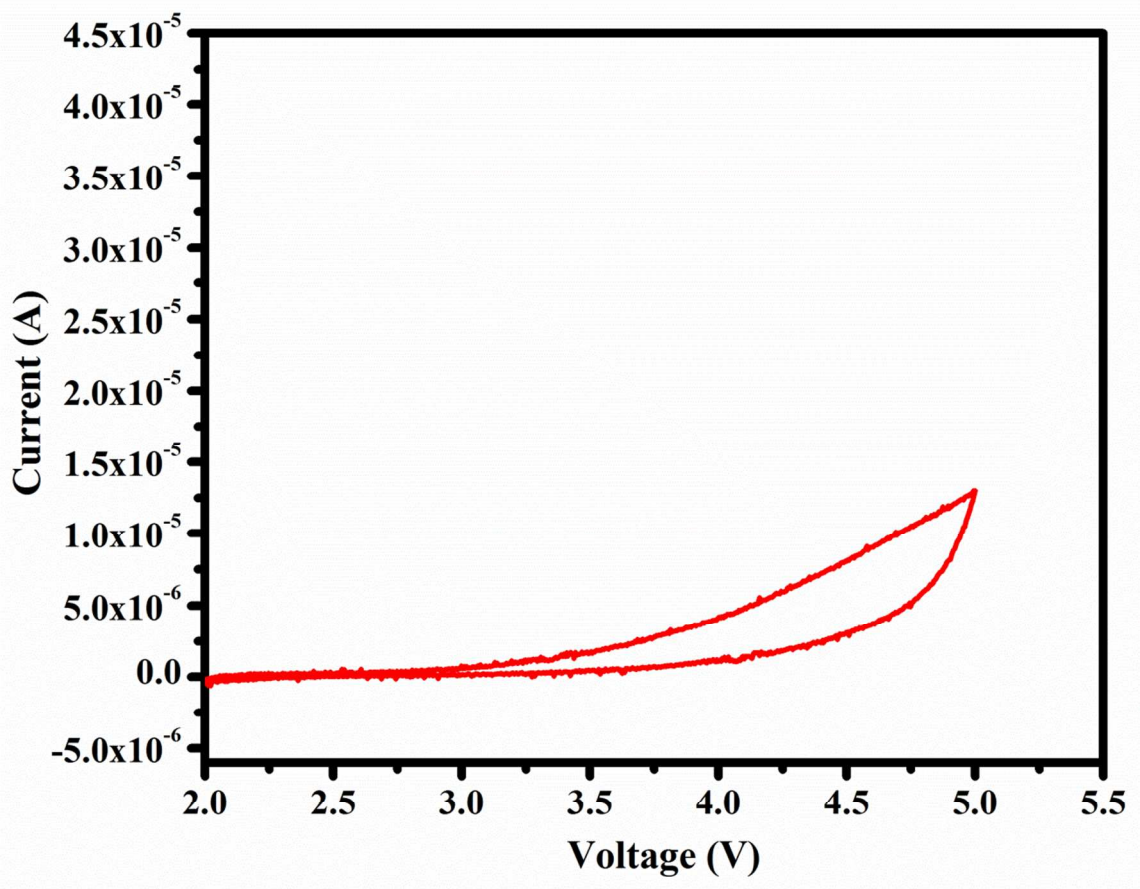

Fig. 8 Potential stability window of the electrospun nanocomposite PMMA blend fibrous electrolyte membrane with 6 wt.% of $ZnAl_2O_4$ fillers content at room temperature.

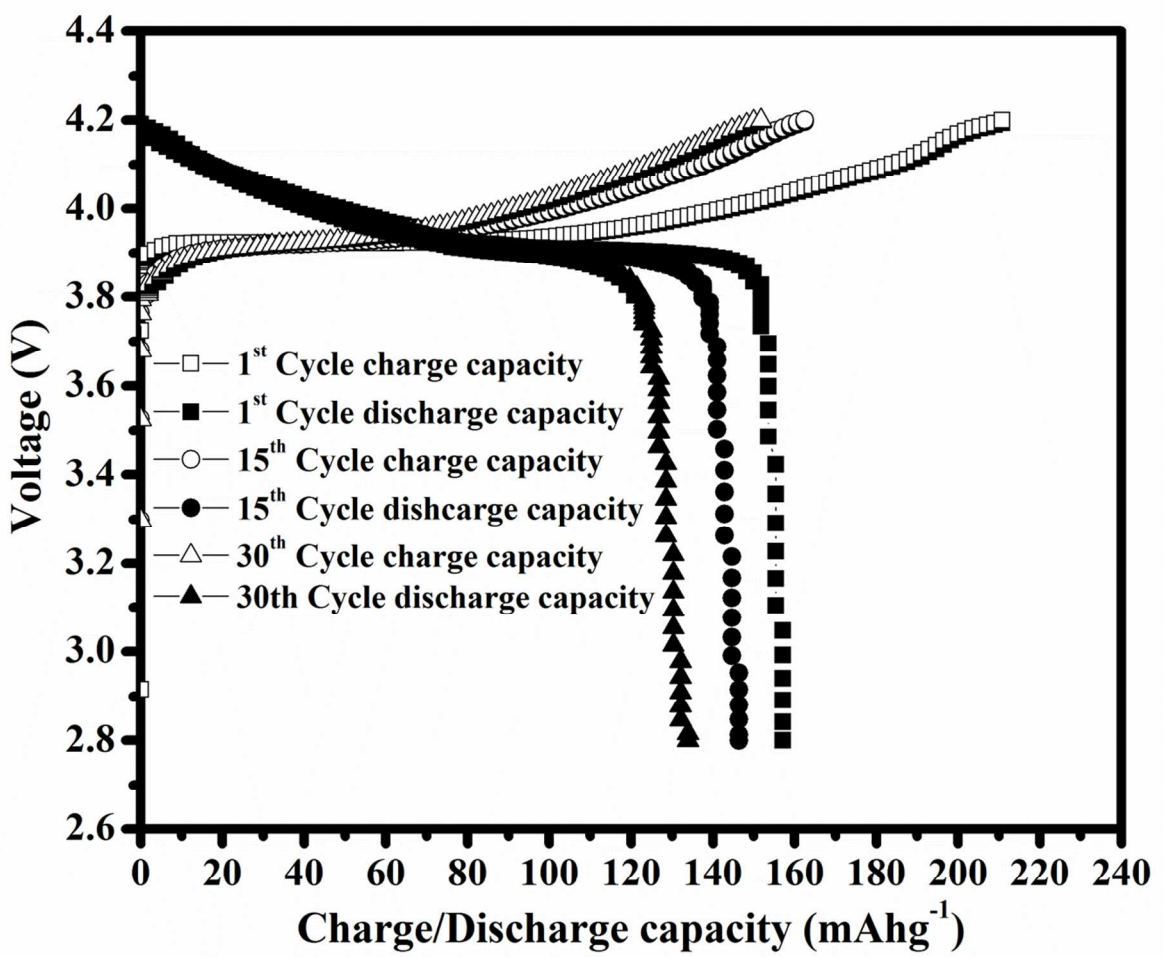

Fig. 9 Charge-discharge capacity of Li/NCPBEs/$LiCoO_2$ CR 2032 coin cell containing the optimized electrospun nanocomposite PMMA blend fibrous electrolyte membrane with 6 wt.% of $ZnAl_2O_4$ fillers content at room temperature.

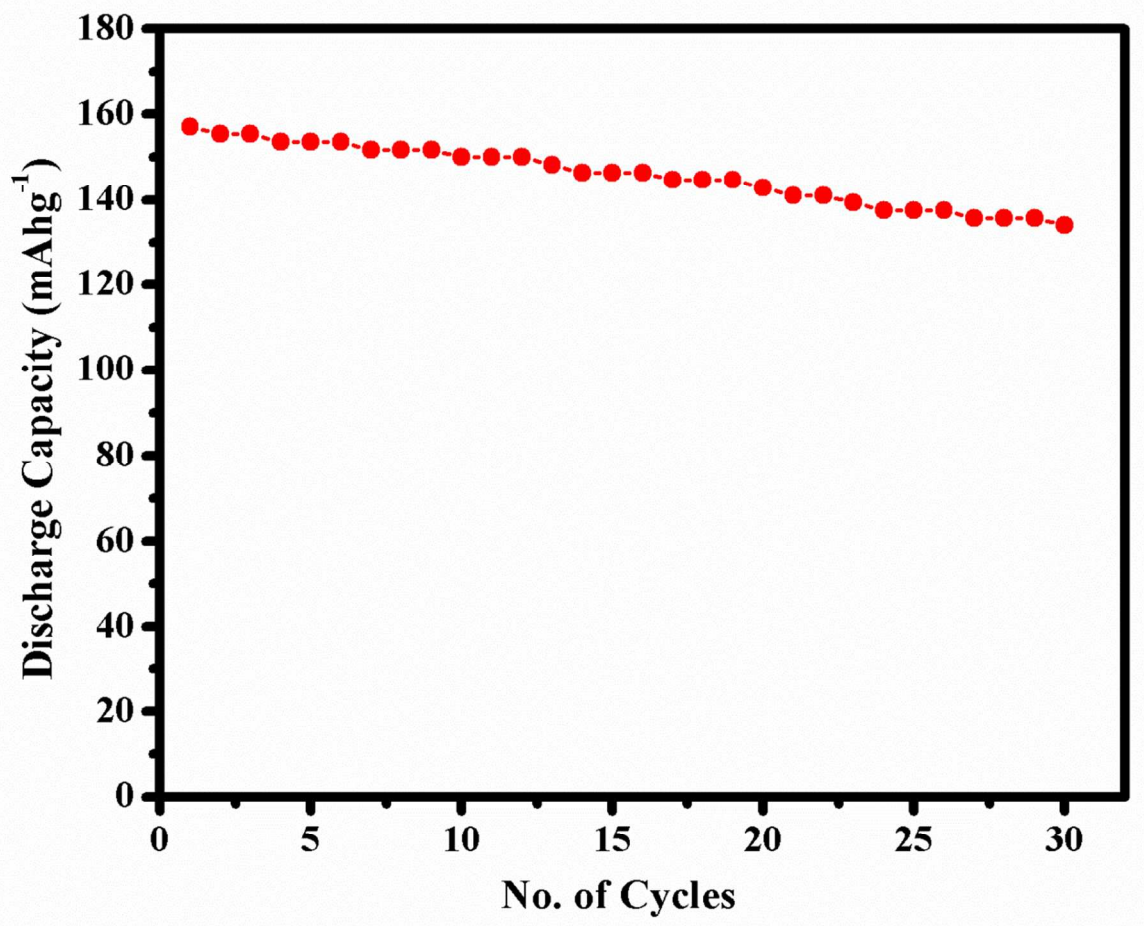

Fig. 10 Cycle performance of Li/NCPBEs/$LiCoO_2$ CR 2032 coin cell containing the optimized electrospun nanocomposite PMMA blend fibrous electrolyte membranes with 6 wt.% of $ZnAl_2O_4$ fillers content at room temperature.

Graphical Abstract